Density Functional Investigation of the Antiferromagnetic Ordering, Spin Orientation, and Ferroelectric Polarization of Rare-Earth Iron Borate $TbFe_3(BO_3)_4$

Changhoon Lee,[†] Jinhee Kang,[†,‡] Kee Hag Lee,*[,‡] and Myung-Hwan Whangbo*[,†]

Department of Chemistry, North Carolina State University, Raleigh, North Carolina 27695-8204, and Department of Chemistry, Nanoscale Science and Technology Institute and BK21, Wonkwang University, Iksan 570-749, Korea

Received March 6, 2009. Revised Manuscript Received April 13, 2009

First-principles density functional calculations were carried out to examine the electronic and magnetic properties of rare-earth iron borate $TbFe_3(BO_3)_4$. The spin exchange interactions between the Fe^{3+} (d^5, $S = 5/2$) ions and the preferred orientation of the Tb^{3+} (f^8) spins were evaluated, and the ferroelectric polarization of $TbFe_3(BO_3)_4$ was calculated. In agreement with experiment, our calculations predict that the spin exchange between the Fe^{3+} spins is ferromagnetic within each //ab sheet of Fe^{3+} ions but antiferromagnetic between adjacent //ab sheets of Fe^{3+} ions, whereas the spin exchange between the Fe^{3+} and Tb^{3+} ions within each //ab sheet of Fe^{3+} and Tb^{3+} ions is antiferromagnetic. The Tb^{3+} (f^8) ions is found to possess an electron configuration responsible for uniaxial magnetism, hence orienting the Tb^{3+} spins along the *c*-direction and leading to the highly anisotropic magnetic susceptibility. The ferroelectric polarization of $TbFe_3(BO_3)_4$ is largely due to the absence of inversion symmetry of the crystal structure and is weakly affected by its magnetic structure.

1. Introduction

Rare-earth iron borates $AFe_3(BO_3)_4$ (A = rare earth) crystallize in the noncentrosymmetric space group $R32$[1,2] and are made of FeO_6 octahedra containing Fe^{5+} ($S = 5/2$, $L = 0$) ions, AO_6 trigonal prisms containing rare-earth A^{3+} ions, and BO_3 triangles. The FeO_6 octahedra share their cis edges to form FeO_4 spiral chains running along the *c*-direction (Figure 1), which are packed by sharing their octahedral corners with AO_6 trigonal prisms and BO_3 triangles (Figure 2) to form the three-dimensional (3D) lattice of $AFe_3(BO_3)_4$. As a result, $AFe_3(BO_3)_4$ consists of trigonal sheets containing the Fe^{3+} and A^{3+} ions in the 3:1 ratio, parallel to the ab-plane (hereafter, the //ab sheets) (Figure 3). Because of the presence of both 3d and 4f magnetic ions, these rare-earth iron borates give rise to interesting and complex magnetic properties.[3−6] In particular, $TbFe_3(BO_3)_4$ undergoes a 3D magnetic ordering at $T_N = 40$ K in which the Fe^{3+} spins have a ferromagnetic (FM) coupling within each //ab sheet (Figure 3), but antiferromagnetic (AFM) coupling between adjacent //ab sheets.[3b] Furthermore, the Tb^{3+} (f^8) spins are antiferromagnetically coupled to the Fe^{3+} spins within each //ab sheet (Figure 3), with their spins oriented along the *c*-direction.[3b] The magnetic ordering of the Tb^{3+} sublattice and that of the Fe^{3+} sublattice set in at the same temperature (i.e., at 40 K). Why $TbFe_3(BO_3)_4$ adopts such a 3D magnetic ordering has not been explained. Furthermore, the magnetic susceptibility of $TbFe_3(BO_3)_4$ is highly anisotropic; the susceptibility perpendicular to the *c*-axis ($\chi_\perp$) is much weaker than that parallel to the *c*-axis ($\chi_{//}$) and is nearly independent of temperature.[3b] This anisotropic magnetism has been ascribed to the Ising-like behavior of the Tb^{3+} ions in the trigonal crystal field.[3] The Ising character, i.e., the uniaxial magnetism, of a magnetic ion arises typically if the ion has a more-than-half-filled shell and if the ion has an electron configuration with three electrons in a doubly degenerate level from the viewpoint of crystal field.[7] Thus, one might speculate that the Tb^{3+} ions of $TbFe_3(BO_3)_4$ possess such an electron configuration. Rare-earth iron borates $AFe_3(BO_3)_4$ have a crystal structure with no inversion symmetry. As a result, $GdFe_3(BO_3)_4$ and $NdFe_3(BO_3)_4$ were found to be multiferroic.[6] In a magnetically driven multiferroic system, the inversion symmetry is removed when it undergoes a magnetic ordering (e.g., spiral spin of cycloid type), thereby inducing ferroelectric (FE) polarization.[8,9] Because $AFe_3(BO_3)_4$ has no inversion symmetry in the crystal

* Corresponding author. E-mail: mike_whangbo@ncsu.edu.
† North Carolina State University.
‡ Wonkwang University.

(1) Hinatsu, Y.; Doi, Y.; Ito, K.; Wakeshima, M.; Alemi, A. *J. Solid State Chem.* **2003**, *172*, 438.
(2) Klimin, S. A.; Fausti, D.; Meetsma, A.; Bezmaternykh, L. N.; van Loosdrecht, P. H. M.; Palstra, T. T. M. *Acta Crystallogr., Sect. B* **2005**, *61*, 481.
(3) (a) Popova, E. A.; Volkov, D. V.; Vasiliev, A. N.; Demidov, A. A.; Kolmakova, N. P.; Gudim, I. A.; Bezmaternykh, L. N.; Tristan, N.; Skourski, Yu.; Buchner, B.; Hess, C.; Klingeler, R. *Phys. Rev. B* **2007**, *75*, 224413. (b) Ritter, C.; Balaev, A.; Vorotynov, A.; Petrakovskii, G.; Velikanov, D.; Temerov, V.; Gudim, I. *J. Phys.: Condens. Matter* **2007**, *19*, 196227. (c) Volkov, D. V.; Popova, E. A.; Kolmakova, N. P.; Demidov, A. A.; Tristan, N.; Skourski, Yu.; Buechner, B.; Gudim, I. A.; Bezmaternykh, L. N. *J. Magn. Magn. Mater.* **2007**, *316*, e717.
(4) (a) Popova, M. N.; Chukalina, E. P.; Stanislavchuk, T. N.; Malkin, B. Z.; Zakirov, A. R.; Antic-Fidancev, E.; Popova, E. A.; Bezmaternykh, L. N.; Temerov, V. L. *Phys. Rev. B* **2007**, *75*, 224435. (b) Tristan, N.; Klingeler, R.; Hess, C.; Buechner, B.; Popova, E.; Gudim, I. A.; Bezmaternykh, L. N. *J. Magn. Magn. Mater.* **2007**, *316*, e621.

10.1021/cm9006475 CCC: $40.75
Published on Web 04/29/2009

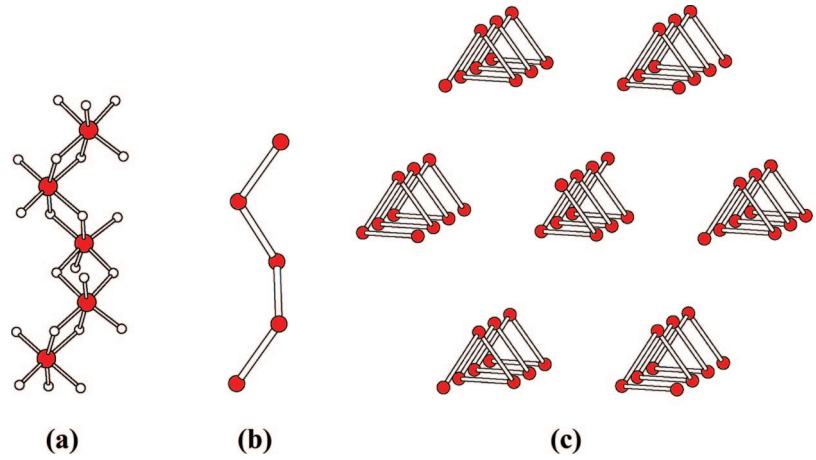

Figure 1. (a) Perspective view of an isolated FeO_4 chain made up of edge-sharing FeO_6 octahedra. (b) Perspective view of an isolated FeO_4 chain showing only the Fe atoms. (c) Packing of the FeO_4 spiral chains in $TbFe_3(BO_3)_4$.

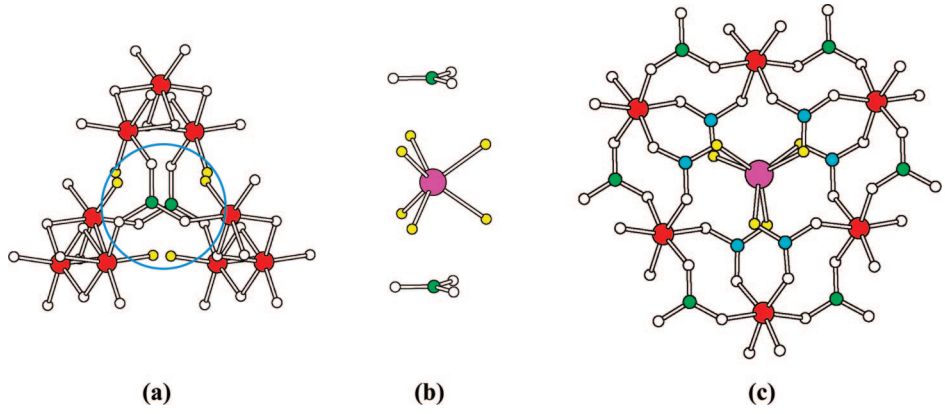

Figure 2. (a) Trigonal prism site for Tb^{3+} generated by three adjacent FeO_4 spiral chains connected by $B(1)O_3$ triangles. (b) Arrangement of a TbO_6 trigonal prism and two adjacent $B(1)O_3$ triangles. (c) Corner-sharing of a TbO_6 trigonal prism, $B(1)O_3$ triangles, $B(2)O_3$ triangles and FeO_6 octahedra. The Tb, B(1), B(2), and Fe atoms are represented by purple, green, cyan, and red circles, respectively.

structure, it would have FE polarization regardless of its magnetic ordering. It is interesting to verify this implication.

To probe the aforementioned issues concerning $TbFe_3(BO_3)_4$, first-principles electronic structure calculations are necessary. In the present work, we investigate these problems on the basis of first-principles density functional theory (DFT) calculations.

2. Crystal Structure and Spin Exchange Paths

A single FeO_4 spiral chain of $TbFe_3(BO_3)_4$ running along the *c*-direction is depicted in Figure 1a. When the structure of each FeO_4 spiral chain is simplified by showing only the Fe atoms (Figure 1b), the arrangement of the FeO_4 spiral chains in $TbFe_3(BO_3)_4$ can be depicted as in Figure 1c. There are two crystallographically different B atoms, i.e., B(1) and B(2). Every three adjacent FeO_4 spiral chains are held together by $B(1)O_3$ triangles, creating trigonal prism sites for the Tb^{3+} ions (Figure 2a). The arrangement of a TbO_6 trigonal prism and two adjacent $B(1)O_3$ triangles is presented in Figure 2b. The FeO_4 spiral chains and the TbO_6 trigonal prisms are also connected by $B(2)O_3$ triangles such that each $B(2)O_3$ triangle shares corners with one TbO_6 trigonal prism and two FeO_4 spiral chains (Figure 2c). Thus, the spin exchange paths to consider between the Fe^{3+} ions of $TbFe_3(BO_3)_4$ include the intrachain superexchange (SE) J_2 as well as the interchain supersuperexchange (SSE) J_1, J_3, and J_4 (Figure 4a). The spin dimer units for J_1-J_4 are depicted in Figure 5, and the geometrical parameters associated with them are summarized in Table 1. Of the three SSE paths, J_4 has the most symmetrically obtuse $\angle Fe-O\cdots O$ angles.

3. Computational Details

To evaluate the spin exchange interactions of $TbFe_3(BO_3)_4$, we carry out first principles DFT electronic structure calculations by employing the frozen-core projector augmented wave method encoded in the Vienna ab initio simulation package (VASP).[10] Our VASP calculations employed the generalized-gradient approximation (GGA)[11] for the exchange-correlation functional, the plane-wave cutoff energy of 400 eV, and 27 k-points for the irreducible Brillouin zone, with the f-electrons of the Tb^{3+} ions treated as core electrons. To describe the possible effect of the strong electron correlation in the Fe 3d states, the GGA plus on-site repulsion U

(5) (a) Balaev, A. D.; Bezmaternykh, L. N.; Gudim, I. A.; Temerov, V. L.; Ovchinnikov, S. G.; Kharlamova, S. A. *J. Magn. Magn. Mater* **2003**, *258−259*, 532. (b) Yen, F.; Lorenz, B.; Sun, Y. Y.; Chu, C. W.; Bezmaternykh, L. N.; Vasiliev, A. N. *Phys. Rev. B* **2006**, *73*, 054435.
(6) Vasiliev, A. N.; Popova, E. A. *Low Temp. Phys.* **2006**, *32*, 735.
(7) (a) Dai, D.; Whangbo, M.-H. *Inorg. Chem.* **2005**, *44*, 4407. (b) Dai, D.; Xiang, H. J.; Whangbo, M.-H. *J. Comput. Chem.* **2008**, *29*, 2187.
(8) Cheong, S.-W.; Mostvoy, M. *Nat. Mater.* **2007**, *6*, 13. (b) Kimura, T. *Annu. Rev. Mater. Res.* **2007**, *37*, 387.
(9) (a) Xiang, H. J.; Whangbo, M.-H. *Phys. Rev. Lett.* **2007**, *99*, 257203. (b) Xiang, H. J.; Wei, S.-H.; Whangbo, M.-H.; Da Silva, J. L. F. *Phys. Rev. Lett.* **2008**, *101*, 037209.

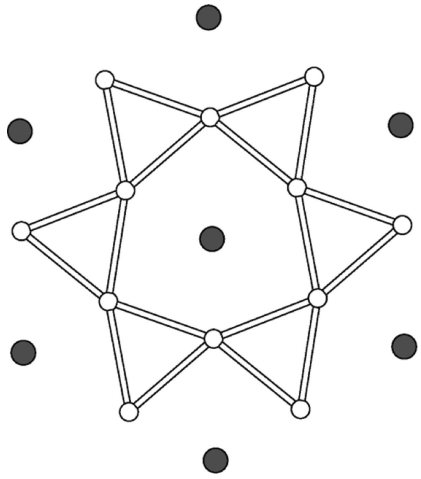

Figure 3. Spin arrangement in a sheet of Fe^{3+} and Tb^{3+} ions parallel to the ab-plane in $TbFe_3(BO_3)_4$. The large and small circles represent the Tb^{3+} and Fe^{3+} ions, respectively. The up-spin and down-spin sites are represented by empty and filled circles, respectively.

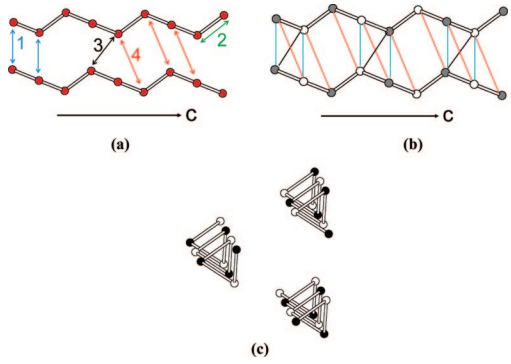

Figure 4. (a) Intrachain and interchain spin exchange paths between the Fe^{3+} ions in $TbFe_3(BO_3)_4$. The numbers 1, 2, 3, and 4 represent J_1, J_2, J_3, and J_4, respectively. (b) Spin exchange interactions between two adjacent FeO_4 spiral chains in the observed magnetic structure, where the filled and empty circles represent up-spin and down-spin Fe^{3+} sites, respectively: J_1 = cyan line, J_2 = white cylinder, J_3 = black line, and J_4 = red line. (c) Spin arrangement in three adjacent FeO_4 spiral chains in the ordered magnetic state of $TbFe_3(BO_3)_4$, where the up-spin and down-spin sites are represented by empty and filled circles, respectively.

(GGA+U) method[12] was employed with effective $U = 5$ eV on the Fe atom. The threshold for the self-consistent-field convergence of the total electronic energy was 1×10^{-6} eV.

We also carried out DFT calculations by using the WIEN2K package[13] so as to treat the f-electrons of the Tb^{3+} ions explicitly and hence evaluate the interactions between the Fe^{3+} and Tb^{3+} ions. Our WIEN2k calculations employed the full-potential linearized augmented plane wave method[14] with the GGA for the exchange-correlation functional, 32 k-points for the irreducible Brillouin zone, the threshold of 1×10^{-6} Ry for the energy convergence, the cutoff energy parameters of $RK_{max} = 5.5$ and $G_{max} = 12$, and the energy threshold of −8.0 Ry for the separation of the core and valence states. To determine the spin orientation of the Tb^{3+} ions, we also performed GGA calculations by taking the effect of spin−orbit coupling (SOC) into consideration.

For various ordered magnetic states (see below) of $TbFe_3(BO_3)_4$, our spin-polarized GGA calculations with both VASP and WIEN2k show that they have a band gap at the Fermi level, in agreement with the fact that $TbFe_3(BO_3)_4$ is a magnetic insulator. As a representative example, the plots of the density of states (DOS) obtained for the FM state of $TbFe_3(BO_3)_4$ from WIEN2k/GGA calculations are presented in Figure 6, which shows that only the up-spin d-block bands of Fe are occupied, as expected for the high-spin Fe^{3+} ions in $TbFe_3(BO_3)_4$. Therefore, in our evaluations of the spin exchange parameters for $TbFe_3(BO_3)_4$, GGA calculations are sufficient. Nevertheless, we carried out GGA+U calculations with $U = 5$ eV by using the VASP to see how GGA+U calculations affect the results of GGA calculations. In GGA+U calculations for magnetic oxides containing Fe, this range of U has been used.[15]

The FE polarization of $TbFe_3(BO_3)_4$ was calculated by using the Berry phase method[16] encoded in the VASP.

4. Spin Exchange Interactions between the Fe^{3+} Ions

To evaluate the four spin exchange parameters J_1−J_4, we perform mapping analysis[17] based on DFT calculations. For this purpose, the relative energies of the five ordered spin states shown in Figure 7 were first determined by GGA+U calculations (Table 2). To extract the values of J_1−J_4 from these electronic structure calculations, we express the total spin exchange interaction energies of the five ordered spin states in terms of the spin Hamiltonian defined in terms of J_1−J_4,

$$\hat{H} = -J_{ij}\hat{S}_i\hat{S}_j \tag{1}$$

where $\hat{S}_i$ and $\hat{S}_j$ are the spin operators at the spin sites i and j, respectively, and J_{ij} (= J_1, J_2, J_3, J_4) is the spin exchange parameter between the sites i and j. By applying the energy expressions obtained for spin dimers with N unpaired spins per spin site (in the present case, $N = 5$),[18] the total spin exchange energies of $TbFe_3(BO_3)_4$ per unit cell (i.e., per three formula units) for the five spin states are written as

$$\begin{aligned} E_{FM} &= (-18J_1 - 9J_2 - 9J_3 - 27J_4)(N^2/4) \\ E_{AF1} &= (-18J_1 - 3J_2 - 3J_3 - 9J_4)(N^2/4) \\ E_{AF2} &= (-10J_1 - 5J_2 - 5J_3 - 15J_4)(N^2/4) \\ E_{AF3} &= (+6J_1 - 3J_2 - 9J_3 + 9J_4)(N^2/4) \\ E_{AF4} &= (+6J_1 - 3J_2 - J_3 + 3J_4)(N^2/4) \end{aligned} \tag{2}$$

Then, by mapping the energy differences between the five ordered states determined from the GGA+U calculations on to the corresponding energy differences determined from the spin Hamiltonian, we obtain the values of J_1−J_4 summarized in Table 3.

(10) (a) Kresse, G.; Hafner, J. *Phys. Rev. B* **1993**, *62*, 558. (b) Kresse, G.; Furthmüller, J. *Comput. Mater. Sci.* **1996**, *6*, 15. (c) Kresse, G.; Furthmüller, J. *Phys. Rev. B* **1996**, *54*, 11169.
(11) Perdew, J. P.; Burke, K.; Ernzerhof, M. *Phys. Rev. Lett.* **1996**, *77*, 3865.
(12) Dudarev, S. L.; Botton, G. A.; Savrasov, S. Y.; Humphreys, C. J.; Sutton, A. P. *Phys. Rev. B* **1998**, *57*, 1505.
(13) Blaha, P.; Schwarz, K.; Madsen, G. K. H.; Kvasnicka, D.; Luitz, J. *WIEN2K, An Augmented Plane Wave + Local Orbitals Program for Calculating Crystal Properties*; Technische Universität Wien: Vienna, Austria, 2001.
(14) Singh, D. J. *Plane Waves, Pseudopotentials and the LAPW Method*; Kluwer Academic: Boston, 1994.
(15) Xiang, H. J.; Wei, S.-H.; Whangbo, M.-H. *Phys. Rev. Lett.* **2008**, *100*, 167207.
(16) (a) King-Smith, R. D.; Vanderbilt, D. *Phys. Rev. B* **1993**, *47*, 1651. (b) Resta, R. *Rev. Mod. Phys.* **1994**, *66*, 899.
(17) (a) Whangbo, M.-H.; Koo, H.-J.; Dai, D. *J. Solid State. Chem.* **2003**, *176*, 417. (b) Xiang, H. J.; Whangbo, M.-H. *Phys. Rev. B* **2007**, *76*, 220411(R). (c) Koo, H.-J.; Whangbo, M.-H. *Inorg. Chem.* **2008**, *47*, 4779.
(18) (a) Dai, D.; Whangbo, M.-H. *J. Chem. Phys.* **2001**, *114*, 2887. (b) Dai, D.; Whangbo, M.-H. *J. Chem. Phys.* **2003**, *118*, 29.

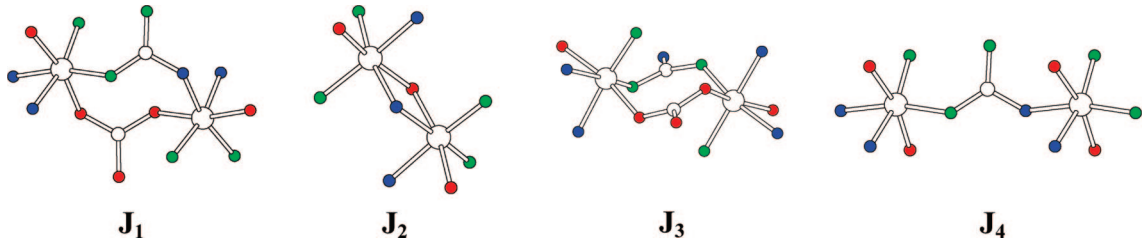

Figure 5. Spin dimers associated with the spin exchange interactions J_1-J_4, where the red, blue, and green circles represent the O(1), O(2), and O(3) atoms, respectively.

Table 1. Geometrical Parameters Associated with the Spin Exchange Paths J_1-J_4 of $TbFe_3(BO_3)_4$

	Fe···Fe (Å)	nature	distance (Å)/angle (deg)
J_1	4.845	SSE	O···O = 2.346 ∠Fe−O···O = 104.7, 146.7 O···O = 2.412 ∠Fe−O···O = 140.4, 106.8
J_2	3.185	SE	∠Fe−O−Fe = 102.9 ∠FeO-Fe = 104.6
J_3	4.375	SSE	O···O = 2.433 ∠Fe−O···O = 110.7, 110.7 O···O = 2.412 ∠Fe−O···O = 106.8, 106.8
J_4	6.065	SSE	O···O = 2.346 ∠Fe−O···O = 144.4, 146.7

Our VASP and WIEN2k calculations both show that all four spin exchange interactions are AFM (Table 3). The VASP calculations reveal that the effect of including the onsite repulsion U on Fe is mainly to decrease the magnitude of each spin exchange interaction, which is expected because the AFM spin exchange is approximately inversely proportional to the onsite repulsion U, namely, $J \approx -(\Delta e)^2/U$, where Δe is the energy split between the two magnetic orbitals describing the spin dimer associated with the spin exchange path J.[17] The strongest AFM interaction is the interchain spin exchange J_4. According to Figure 4b, the experimentally observed AFM arrangement of the Fe^{3+} ions in $TbFe_3(BO_3)_4$ is favored by J_2, J_3, and J_4, but disfavored by J_1. Note that J_2, J_3, and J_4 are all interactions between adjacent //ab sheets, whereas J_1 is an interaction within //ab sheet. J_2 is an intrachain interaction, whereas J_3 and J_4 are interchain interactions. J_1 is much weaker

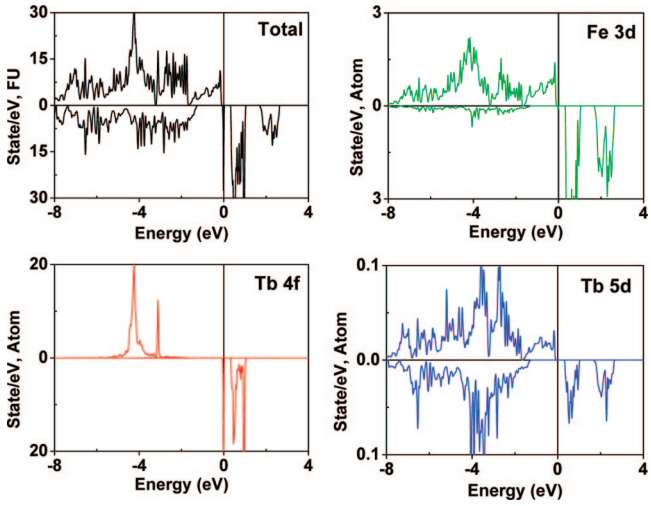

Figure 6. Electronic structure obtained for the ferromagnetic state of $TbFe_3(BO_3)_4$ from WIEN2k/GGA calculations: The total DOS plot as well as the projected DOS plots for the Fe 3d, the Tb 4f,and the Tb 5d states.

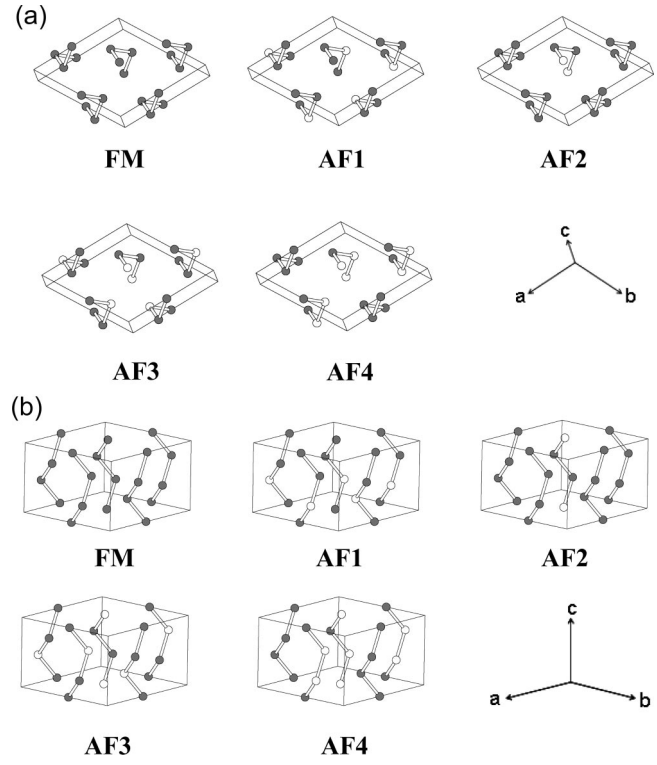

Figure 7. Two perspective views of the five ordered spin states (FM, AF1, AF2, AF3, and AF4) of $TbFe_3(BO_3)_4$, where the up-spin and down-spin Fe^{3+} sites are represented by empty and filled circles, respectively.

Table 2. Relative Energies ΔE (in meV) of the Five Ordered Spin States of $TbFe_3(BO_3)_4$ per Unit Cell (i.e., per three formula units) Obtained from GGA+U Calculations

	VASP		WIEN2k
state	$U = 0$ eV	$U = 5$ eV	$U = 0$ eV
FM	0	0	0
AF1	−630	−205	−640
AF2	−262	−78	−264
AF3	−735	−224	−741
AF4	−590	−168	−605

Table 3. Spin Exchange Parameters J/k_B (in K) of $TbFe_3(BO_3)_4$ Determined from GGA+U Calculations

	VASP		WIEN2k
	$U = 0$ eV	$U = 5$ eV	$U = 0$ eV
J_1/k_B	−12.0	−2.2	−11.7
J_2/k_B	−7.0	−1.3	−12.7
J_3/k_B	−7.7	−1.5	−7.7
J_4/k_B	−27.6	−9.6	−26.2

than J_4 (e.g., $J_1/J_4 \approx 0.23$ with $U = 5$ eV), and more J_4 interactions occur than do J_1 interactions between adjacent FeO_4 spiral chains (by a factor of 1.5). Namely, the magnetic structure

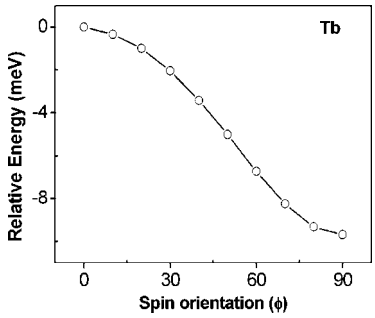

Figure 8. Relative energy of $TbGa_3(BO_3)_4$ per unit cell (i.e., three formula units) determined from GGA+SOC calculations as the orientation angle ϕ of the Tb^{3+} spin sweeps from 0° (//a) to 90° (//c) in the ac-plane.

of $TbFe_3(BO_3)_4$ has practically no geometric spin frustration,[19] and the FM coupling between the Fe^{3+} spins within each //ab sheet is a consequence of the fact that the Fe^{3+} spins have a strong AFM coupling between adjacent //ab sheets through the interchain spin exchange J_3 and J_4. This explains why the Curie−Weiss temperature $\theta_{//}$ determined from the parallel susceptibility $\chi_{//}$ of $TbFe_3(BO_3)_4$ is very close to the Néel temperature T_N (i.e., 50 vs 40 K).

5. Orientation of Tb^{3+} Spin and Interaction between the Tb^{3+} and Fe^{3+} Sublattices

The orientation of a spin at a given atomic site is determined by SOC, which is local in nature.[7b] Therefore, in determining the orientation of the Tb^{3+} spin in $TbFe_3(BO_3)_4$ by GGA+SOC calculations, it is sufficient to consider the hypothetical crystal structure $TbGa_3(BO_3)_4$, which results from $TbFe_3(BO_3)_4$ when the magnetic Fe^{3+} ions are replaced with diamagnetic Ga^{3+} ions. Here, Ga^{3+} ions are chosen because the ionic radius of Ga^{3+} at a six-coordinate site is close to that of high-spin Fe^{3+} at a six-coordinate site (0.62 vs 0.645 Å).[20] (A similar approach was used in determining the orientation of the Tb^{3+} spin in $TbMnO_3$.[9b]) Our GGA+SOC calculations for $TbGa_3(BO_3)_4$ were carried out as a function of the orientation of the Tb^{3+} spins, which we sweep in the ac-plane from the *a*-axis (the sweep angle $\phi = 0°$) to the *c*-axis ($\phi = 90°$). The calculated energy of $TbGa_3(BO_3)_4$ as a function of ϕ is plotted in Figure 8, which predicts that the Tb^{3+} spin should be parallel to the *c*-axis in agreement with experiment. The calculated spin and orbital moments of Tb^{3+} are 5.78 and 0.97 μ_B, respectively, at $\phi = 90°$, and 5.78 and 0.93 μ_B, respectively, at $\phi = 0°$.

To account for why the Tb^{3+} (f^8) spin prefers the //c orientation, we note that each TbO_6 trigonal prism of $TbFe_3(BO_3)_4$ has a 3-fold rotational symmetry (Figure 2), so the crystal field splitting of the Tb 4f levels leads to doubly degenerate states. Indeed, the projected DOS plots calculated for the Tb 4f states (Figure 9) reveal that each of the $m_l = \pm1$, ±2, and ±3 substates appears as a doubly degenerate level. As expected for an f^8 ion, all up-spin levels are occupied. The remaining one down-spin f-electron is found at the level given by a linear combination of the $m_l = 0$ and

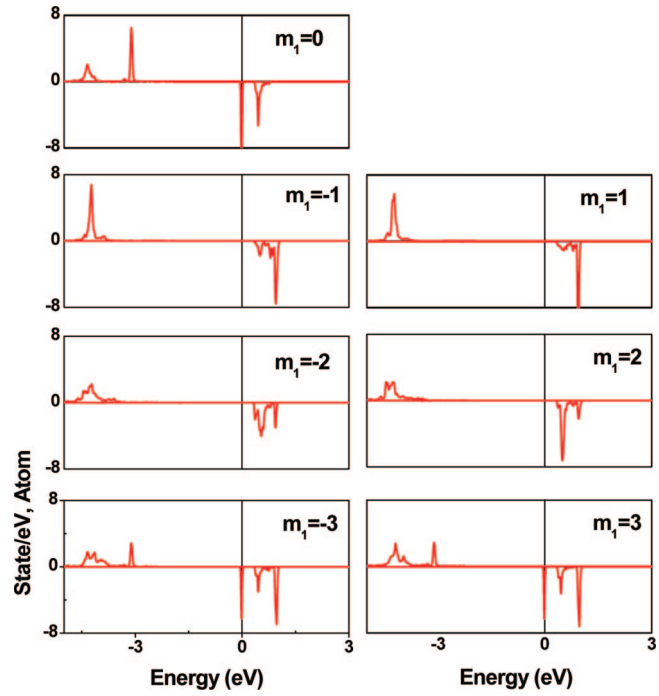

Figure 9. Projected DOS plots calculated for the $m_l = 0$, ±1, ±2, and ±3 states of Tb^{3+} determined from WIEN2k/GGA+SOC calculations for the magnetic ground state of $TbGa_3(BO_3)_4$, in which the Tb^{3+} spin has the //c direction.

$m_l = \pm3$ states (Figure 9). In other words, from the viewpoint of the crystal field, the doubly degenerate $m_l = \pm3$ level is occupied by more than two electrons. Consequently, this electron configuration should give rise to a uniaxial magnetism for the Tb^{3+} ions and hence the preference for the Tb^{3+} spin to orient along the 3-fold rotational axis (i.e., the //c direction) by analogy with the uniaxial magnetism found for high-spin Fe^{2+} (d^6) ions at linear two-coordinate and trigonal-prism six-coordinate sites.[7] This conclusion is consistent with the Ising-like behavior of the magnetic properties of $TbFe_3(BO_3)_4$.[3,4]

To examine the interaction between the Tb^{3+} and Fe^{3+} sublattices, we consider the two ordered spin arrangements of the Tb^{3+} ions with respect to the observed AFM arrangement of the Fe^{3+} ions: (a) In each //ab sheet of Fe^{3+} ions, the Tb^{3+} spins are FM to the Fe^{3+} spins (i.e., the Tb/Fe FM-arrangement). (b) In each //ab sheet of Fe^{3+} ions, the Tb^{3+} spins are AFM to the Fe^{3+} spins (i.e., the Tb/Fe AFM-arrangement). Our GGA calculations show that the Tb/Fe AFM-arrangement is substantially more stable than the Tb/Fe FM-arrangement (by ~6 meV per Tb^{3+}). The preference for the Tb/Fe AFM arrangement is in agreement with experiment.[3b] The substantial preference for the Tb/Fe AFM arrangement means that the Tb^{3+} sublattice interacts strongly with the Fe^{3+} sublattice. This explains why the magnetic ordering of the Tb^{3+} sublattice and that of the Fe^{3+} sublattice occur simultaneously at the same temperature (i.e., at 40 K).

It is of importance to consider why the spin exchange between adjacent Fe^{3+} (d^5) and Tb^{3+} (f^8) ions in the //ab sheet (see Figures 2c and 3) is AFM. Concerning the spin exchange between rare-earth and transition metal magnetic

(19) (a) Greedan, J. E. *J. Mater. Chem.* **2001**, *11*, 37. (b) Dai, D.; Whangbo, M.-H. *J. Chem. Phys.* **2004**, *121*, 672.
(20) Shannon, R. D. *Acta Crystallogr., Sect. A* **1976**, *32*, 751.

ions, several mechanisms have been considered.[21] Roy and Hughbanks have shown that the spin exchange between adjacent Gd^{3+} (f^7) ions in Gd-containing molecules and solids is mediated by the 5d orbitals of Gd^{3+}.[22] This finding should be valid for the spin exchange of other rare-earth ions as well, because their 4f orbitals are too contracted to participate in SE and SSE interactions. Thus, the AFM spin exchange between adjacent Tb^{3+} (f^8) and Fe^{3+} (d^5) ions in $TbFe_3(BO_3)_4$ leads to two implications. The first is that the spin exchange of the Tb^{3+} 5d orbitals with the Fe^{3+} 3d orbitals should be AFM. This is most likely the case because this exchange, which occurs through the BO_3 bridges (Figure 2c), is of SSE type.[17a] The second implication is that from the viewpoint of atomic electronic structure, the $4f^8$ configuration of Tb^{3+} should be close in energy to its excited configuration $4f^75d^1$. Equivalently, from the viewpoint of electronic structure calculations for $TbFe_3(BO_3)_4$, the population of the Tb^{3+} 5d orbitals should be nonzero hence leading to the "fractional d electron" on Tb^{3+}. The latter is indeed the case, as can be seen from the projected DOS plot for the 5d orbitals of Tb^{3+} (Figure 6). When these two conditions are met, the AFM coupling between adjacent Tb^{3+} (f^8) and Fe^{3+} (d^5) ions is determined by the SSE interaction of the "fractional d electron" of Tb^{3+} with the d electrons of Fe^{3+}, while the f electrons of a Tb^{3+} site become ferromagnetically coupled to the "fractional d-electron" at the same Tb^{3+} site because of Hund's rule. As a consequence, the spin exchange between the Tb^{3+} (f^8) and Fe^{3+} (d^5) ions is AFM.

Finally, we comment on $NdFe_3(BO_3)_4$, which is isostructural with $TbFe_3(BO_3)_4$ and undergoes a 3D magnetic ordering below 30.5 K in which the Fe^{3+} spins are ferromagnetically coupled within each //ab sheet but those of adjacent //ab-plane sheets are antiferromagnetically coupled.[23] These aspects are similar to those found for $TbFe_3(BO_3)_4$. However, the spin orientation of $NdFe_3(BO_3)_4$ differs from that of $TbFe_3(BO_3)_4$; in each //ab sheet the Fe^{3+} and Nd^{3+} (f^3) spins are parallel to the ab-plane, but the Fe^{3+} spins are orthogonal to the Nd^{3+} spins.[23] Results of our study on $NdFe_3(BO_3)_4$ will be reported elsewhere.[24]

6. Ferroelectric Polarization

We calculated the FE polarization of $TbFe_3(BO_3)_4$ for the observed AFM state of the Fe^{3+} ions to find that the polarization is zero along the *c*-direction ($P_{//c} = 0$), and 3.72 $\mu C/m^2$ perpendicular to the *c*-direction ($P_\perp = 3.72\ \mu C/m^2$). For the hypothetical FM state of the Fe^{3+} ions, in which the Fe^{3+} spins have an FM coupling not only within each //ab sheet but also between adjacent //ab sheets, our calculation gives $P_{//c} = 0$ and $P_\perp = 3.12\ \mu C/m^2$. Thus, the effect of the magnetic structure on the FE polarization of $TbFe_3(BO_3)_4$ is very weak, and the small FE polarization calculated for $TbFe_3(BO_3)_4$ arises primarily from the fact that its crystal structure has no inversion symmetry regardless of the magnetic structure.

7. Concluding Remarks

The magnetic structure predicted for $TbFe_3(BO_3)_4$ from our DFT calculations are in good agreement with experiment. The Fe^{3+} spins have a FM coupling within each //ab sheet but AFM coupling between adjacent //ab sheets, largely due to the strong interchain AFM spin exchange J_4. The Tb^{3+} (f^8) ions at the trigonal prism sites have an electron configuration leading to uniaxial magnetism, so that the Tb^{3+} spins orient along the *c*-direction and the magnetic susceptibility of $TbFe_3(BO_3)_4$ is highly anisotropic. The Tb^{3+} spins have a substantial AFM coupling to the Fe^{3+} ions within each //ab sheet, which explains why the Tb^{3+} and Fe^{3+} spins order at the same temperature. The FE polarization of $TbFe_3(BO_3)_4$, arising from the absence of inversion symmetry in the crystal structure, is small and only weakly affected by the magnetic structure of $TbFe_3(BO_3)_4$.

Acknowledgment. This work was supported by the Office of Basic Energy Sciences, Division of Materials Sciences, U.S. Department of Energy, under Grant DE-FG02-86ER45259, and by the resources of the NERSC Center supported under Contract DE-AC02-05CH11231. J.H.K. and K.H.L. are grateful for the support from the Korea Research Foundation Grant (MOEHRD, KRF-2007-612-C00036, and KRF-2007-313-C00332).

CM9006475

(21) Benelli, C.; Gatteschi, D. *Chem. Rev.* **2002**, *102*, 2369.

(22) (a) Roy, L. E.; Hughbanks, T. *Mater. Res. Soc. Symp. Proc.* **2002**, *755*, 25. (b) Roy, L.; Hughbanks, T. *J. Solid State Chem.* **2003**, *176*, 294. (c) Roy, L. E.; Hughbanks, T. *J. Am. Chem. Soc.* **2006**, *128*, 568. (d) Sweet, L. E.; Roy, L. E.; Meng, F.; Hughbanks, T. *J. Am. Chem. Soc.* **2006**, *128*, 10193. (e) Roy, L.; Hughbanks, T. *J. Phys. Chem. B* **2006**, *110*, 20290.

(23) Fischer, P.; Pomjakushin, V.; Sheptyyakov, D.; Keller, L.; Janoschek, M.; Roessli, B.; Schefer, J.; Petrakovskii, G.; Bezmaternikh, L.; Temerov, V.; Velikanov, D. *J. Phys.: Condens. Matter* **2006**, *18*, 7975.

(24) Lee, C.; Kang, J.; Lee, K. H.; Whangbo, M.-H. To be published.